minerals

MDPI

Article

Extraction and Interpretation of Gold Exploration Indexes in Jinya-Mingshan Area Based on Association Rule Algorithm and Statistical Analysis

Xinzhu Dong, Guangfei Guo *, Yang Huang, Weihe Chen, Zhiyuan Ni, Jiandong Meng and Pingru Li

Haikou Marine Geological Survey Center, China Geological Survey, Haikou 571127, China; rqwso@126.com (X.D.); hymovingon@mail.hnust.edu.cn (Y.H.); chenweihe@mail.cgs.gov.cn (W.C.); nizhiyuan@mail.cgs.gov.cn (Z.N.); 17589768981@163.com (J.M.); lipingru@mail.cgs.gov.cn (P.L.)
* Correspondence: ggf@mail.cgs.gov.cn

Abstract: Geochemical data serve as crucial references for prospecting, and the effective extraction of prospecting information from such data determines the success rate of exploration. In the era of big data, novel prospecting methods based on geochemical data offer new ideas for exploring various ore deposits. By employing advanced data analysis techniques like machine learning and artificial intelligence, it becomes possible to identify elusive patterns and trends that are challenging to detect using traditional approaches, thereby significantly enhancing the success rate of prospecting endeavors. In this study, we selected drainage sediment geochemical data (Au, Ba, Mo, Sb, V, W, Zn) in the Jinya-Mingshan area to explore potential Carlin-type gold deposits. Traditional geochemical processing methods along with an association rule algorithm were employed for conducting comprehensive data mining analysis. The results demonstrate that the element combinations within the study area can be categorized into strong positive associations and enrichments (Mo, Sb, Zn) associated with vulcanization, strong negative associations, and decarbonation-related migration elements (Ba), as well as strong positive associations and weakly enriched elements (W) and weak positive associations and weakly enriched elements (V) not significantly related to mineralization. In comparison to Mo and Sb, which are closely linked to Au as revealed by cluster analysis and factor analysis, the association rule algorithm also reveals a relatively close correlation between Ba, Zn, and Au. Based on the element correlations obtained through the association rule algorithm, a new prospecting index was constructed for the study area. This new index is more reasonable than traditional indices. In conclusion, the association rule algorithm possesses unique advantages in information mining of geochemical data and holds promising applications in geological exploration.

Keywords: gold deposit; association rule algorithm; statistical analysis; indicator extraction

check for updates

Academic Editor: Paul Alexandre

Received: 26 December 2024
Revised: 25 January 2025
Accepted: 1 February 2025
Published: 11 February 2025

Citation: Dong, X.; Guo, G.; Huang, Y.; Chen, W.; Ni, Z.; Meng, J.; Li, P. Extraction and Interpretation of Gold Exploration Indexes in Jinya-Mingshan Area Based on Association Rule Algorithm and Statistical Analysis. *Minerals* **2025**, *15*, 165. https://doi.org/10.3390/min15020165

Copyright: © 2025 by the authors. Licensee MDPI, Basel, Switzerland. This article is an open access article distributed under the terms and conditions of the Creative Commons Attribution (CC BY) license (https://creativecommons.org/licenses/by/4.0/).

1. Introduction

The Jinya-Mingshan area is situated in the eastern part of the Youjiang Basin (Figure 1), which represents a significant Carlin-type gold accumulation zone. This region has witnessed the discovery of two major Carlin-type gold deposits, namely Jinya and Mingshan, along with several smaller ones like Luolou. Recent exploration efforts have revealed the presence of additional gold deposits in this area, indicating promising prospects for further exploration activities. Extensive research on the genesis of typical gold deposits within the Jinya-Mingshan area has been conducted by previous scholars, leading to a

comprehensive understanding of its fundamental geological characteristics, ore-forming processes, source materials for mineralization, evolution of ore-forming fluids, and deposit genetic models [1–3]. Given the large-scale prospecting endeavors undertaken in this region, earlier studies primarily focused on conducting 1:50,000 geological minerals and stream sediment surveys to obtain abundant geological data and geochemical information (elemental contents). However, these geochemical datasets were subjected only to simple single-element anomaly analysis and qualitative assessments regarding multi-element anomaly superposition as one of the prospecting indicators employed during exploration work. Nevertheless, it should be noted that such geochemical data often exhibit complex structures due to their substantial quantity and potential influence from multi-stage geological processes. The simple qualitative analysis of anomalies poses challenges in fully extracting and integrating the hidden information from different elements, thereby limiting the efficiency of utilizing geochemical data and hindering the extraction of effective geochemical exploration indices. To address this issue, some approaches that simplify data for descriptive, interpretive, and analytical purposes have been explored in analyzing geochemical data, such as principal component analysis and factor analysis [4,5]. In recent years, with the rapid advancements in machine learning technology and algorithms, it has demonstrated significant advantages in deep mining complex information from massive datasets. Consequently, an increasing number of geologists are adopting these cutting-edge technologies within the field of geoscience prospecting to provide novel methods and ideas [6–8].

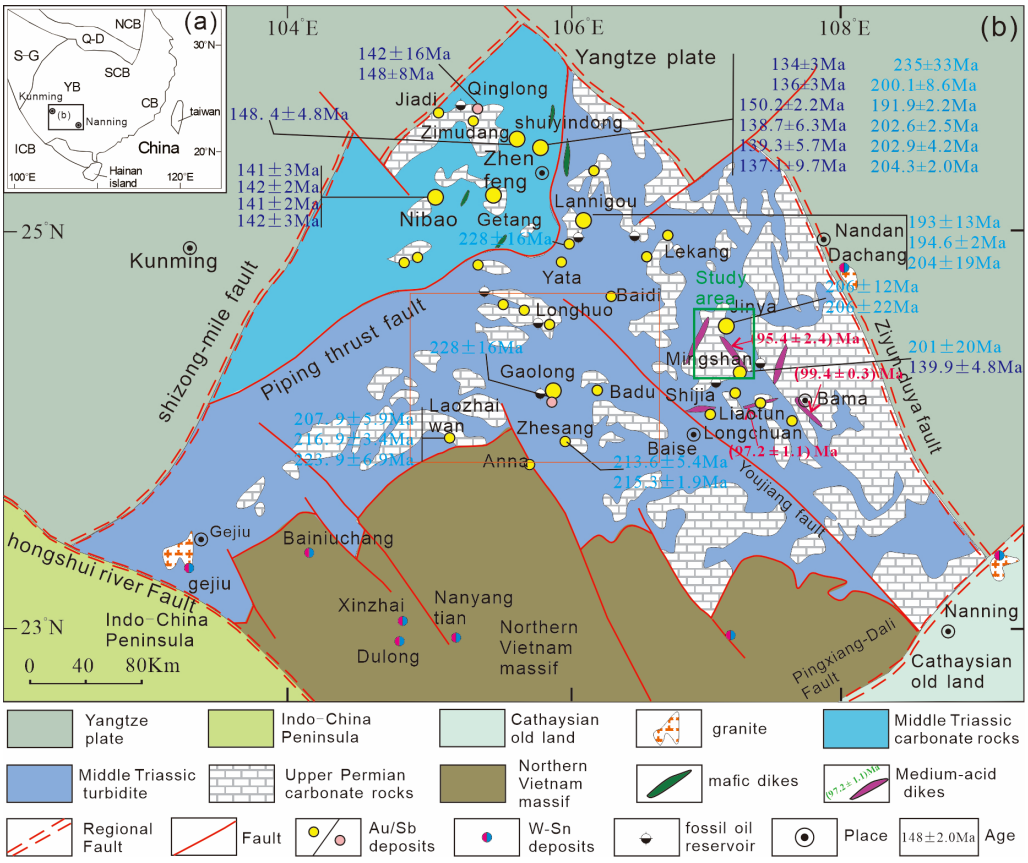


Figure 1. The location of the Youjiang Basin (**a**), distribution of Carlin-type gold deposits in Youjiang Basin (**b**) (modified from [9,10]).

The application of machine learning techniques (e.g., random forest, neural network, association rules) for extracting geochemical characteristics and conducting information

fusion can yield more efficient exploration indicators compared to element anomalies alone. As a result, it greatly enhances the effectiveness of deep exploration in concealed areas [11–13].

This paper focuses on the gold deposit in the Jinya-Mingshan area as the research subject. Based on the geochemical data of drainage sediments in this region, a combination of traditional statistical analysis methods (such as cluster analysis and factor analysis) and machine learning techniques (specifically association rule algorithm) is employed to extract exploration indicators for gold deposits. Additionally, by integrating fundamental geological and mineral data along with previous research findings on typical deposits, we interpret the results obtained from the association rule algorithm and evaluate the effectiveness of exploration indicators derived through machine learning methods, aiming to provide guidance for gold exploration efforts in this area. Specifically, cluster analysis is primarily utilized for element classification, factor analysis emphasizes overall element correlations, while association rules algorithm focuses on local element correlations [11].

2. Materials and Methods

2.1. The Geological Background of the Study Area

The study area is situated in the eastern part of Youjiang Basin (Figure 1), which represents the second largest Carlin-type gold deposit region globally. A number of Carlin-type gold occurrences, such as Baye and Linlaoping, have also been reported in the study area. Notably, within Youjiang Basin, there exist several significant to superlative gold deposits such as Quicksilver Cave, Mudbao, and Mudgou, with proven gold reserves amounting to nearly 1000 tons [13]. Due to its association with the evolutionary processes of both the Triassic Tethys Ocean and Cretaceous Paleo-Pacific Ocean, this basin exhibits extensive occurrences of carbonate rocks and fine clastic sedimentary rocks, thereby providing favorable geological conditions for gold mineralization [14].

The study area is situated in the eastern part of Youjiang Basin, where two significant gold deposits, namely Jinya and Mingshan, are present (Figure 1). The geological formations within the study area comprise Carboniferous Du'an Formation, Dapu Formation, Huanglong Formation, Carboniferous Permian Ma Ping Formation, Permian Qixia Formation, Maokou Formation and Heshan Formation, as well as Triassic Luolou Formation, Baifeng Formation, Banna Formation and Lanmu Formation (Figure 2). The lithology of Carboniferous Permian formation is predominantly characterized by carbonate rocks while that of Triassic formation consists mainly of fine clastic rocks such as mudstone, siltstone and sandstone. Generally speaking, the strata exhibit a northwest trend with only a few late Cretaceous quartz porphyry dikes observed in the study area which are oriented towards the northwest or northeast directions. These dikes are primarily located near Mingshan gold deposit with some spatial association between dike rocks and gold ore bodies [1]. Fault structures are extensively developed within the study area, including syndepositional faults occurring between Permian carbonate rocks and Triassic fine clastic rocks; these faults display relatively complex orientations. Additionally, other faults mainly trend towards NNW and NW directions (Figure 2). Folds also exhibit considerable development within the study area with their axes generally trending towards NNW direction. These folds result in repeated occurrences of identical strata multiple times in the northeastern direction (Figure 2). In the study area, alteration processes such as decarbonation, argillation, silicification, and limonization have been observed predominantly within the fracture zone. The mineral assemblage in this region primarily consists of gold deposits alongside significant occurrences of antimony deposits, copper deposits (deposits), pyrite, and limonite deposits. Notably, certain antimony deposits exhibit a close association with gold deposits (Figure 2). Gold mineralization (points) is mainly hosted within Triassic fine clastic rocks exhibiting a

spatial distribution closely associated with fault structures. Surrounding rock alteration is characterized by silicification, pyritization, argillization, and decarbonation. Within typical gold deposits (Jinya and Mingshan gold deposits), gold occurs predominantly as fine invisible particles within pyrite and arsenopyrite.

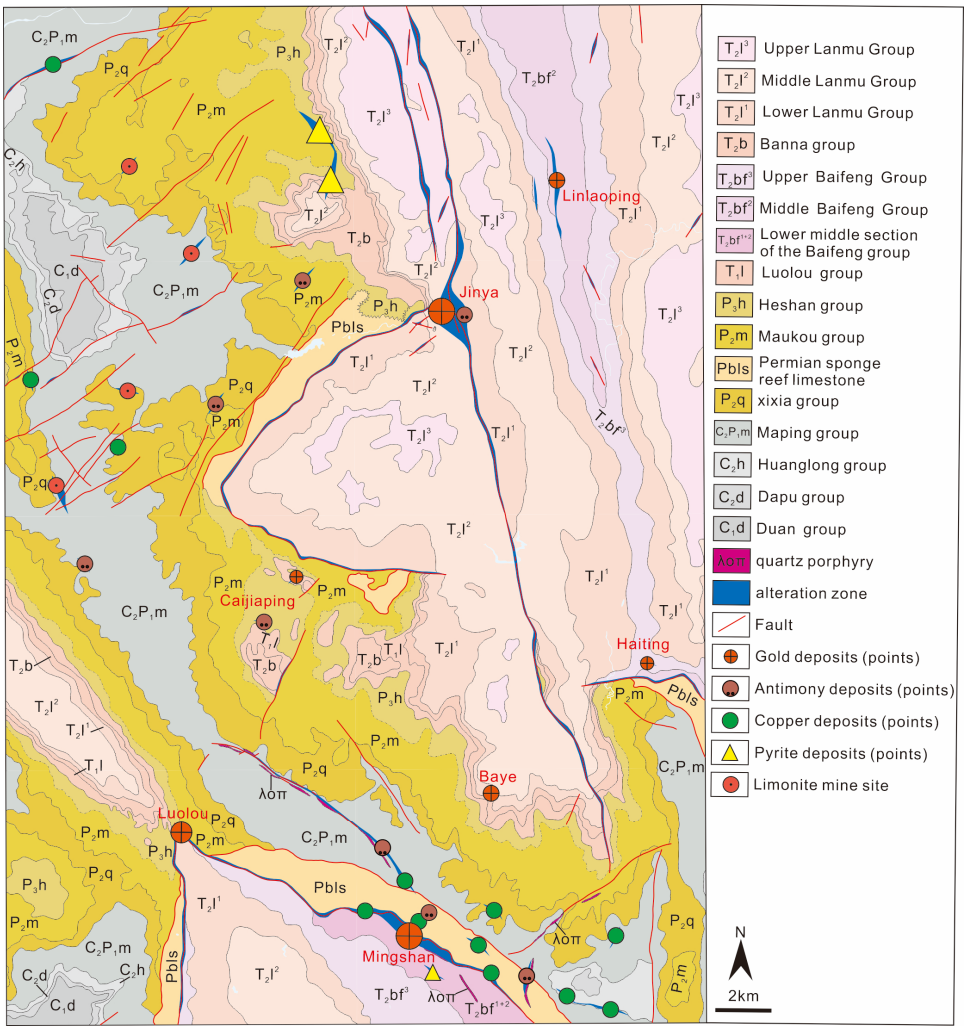


Figure 2. Geological map of the Jinya-Mingshan area.

2.2. Research Methods and Principles

2.2.1. Cluster Analysis and Factor Analysis

Cluster analysis aims to group objects in a dataset into clusters based on their similar characteristics, thereby facilitating the identification of patterns and structures within the data. Various clustering methods are employed for this purpose, including K-means clustering, hierarchical clustering, fuzzy clustering, etc. [15]. Among these methods, K-means clustering is a prevalent unsupervised learning algorithm utilized for grouping observations into distinct clusters within a dataset [16]. The steps involved in K-means clustering can be categorized as the four components shown in Table 1. Ultimately, each data point belongs to a specific cluster based on this process.

The concept of factor analysis was initially introduced by Charles Spearman in 1904 as a technique for simplifying and reducing the dimensionality of data. By examining the inherent relationships among multiple variables, it uncovers the fundamental structure of observed data and represents this structure using a limited number of "abstract" variables known as factors. These factors encapsulate much of the information contained within the original variables. Factor analysis elucidates intricate associations between multiple

variables through a small set of common factors. It decomposes each original variable into two components: one comprises shared common factors across all variables, while the other encompasses unique factors specific to each individual variable, thereby distinguishing them from one another. As an essential method in multivariate statistical analysis, factor analysis has gained widespread adoption in geoscience research in recent years. It enables integration of numerous geochemical variables into a few common factors that can serve as potential indicators for metallogenic prediction [11,17].

Table 1. The four steps of the K-means clustering algorithm.

Step Number	Operation
Initialization	Selecting K initial centroid points either randomly or using heuristic techniques
Allocation	Calculating the distance between each data point and every centroid to assign it to the nearest cluster
Updating centroids	Computing the mean of all members within each cluster and updating the centroid accordingly
Stop	Repeating steps 2 and 3 until convergence or reaching a predetermined number of iterations

2.2.2. Association Rule Algorithm

The association rule algorithm is a widely used technology in data mining, primarily employed to discover the associations between items within a dataset [18]. Its fundamental concepts include an item (an individual element within the dataset), a transaction (a record comprising multiple items), and a frequent item set (a collection of items that appear frequently within the dataset). The classic algorithm for association rule mining, namely the Apriori algorithm, can be divided into two main steps: (1) generation of frequent item sets, and (2) generation of association rules. Amongst numerous generated association rules, identifying effective ones necessitates evaluating their validity indicators. Commonly employed evaluation metrics for association rules include support and confidence. Figure 3 illustrates the workflow diagram of association rule mining.

The following is an example of the meaning of the main indicators in association rules. For association rules $A \rightarrow B$, where A is the antecedent and B is the consequent.

The rule's support is $S_{A \rightarrow B} = P(A \cap B)$, representing the probability of co-occurrence. $S_A = P(A)$ and $S_B = P(B)$ correspond to the support of the antecedent and consequent, respectively.

Rule confidence (confidence) is $C_{A \rightarrow B} = \frac{S_{A \rightarrow B}}{S_A} = \frac{P(A \cap B)}{P(A)} = P(B|A)$, that is the conditional probability of event B given the occurrence of event A.

In practical applications, a strong association rule generally necessitates high levels of both support and confidence; thus, it is customary to set smaller thresholds for these measures. The validity of an association rule is contingent upon the simultaneous satisfaction of both $S_{A \rightarrow B} \geq S_{min}$ and $C_{A \rightarrow B} \geq C_{min}$. Based on the definitions of support and confidence, it can be conclusively inferred that $C_{A \rightarrow B} \geq S_{A \rightarrow B}$ holds. If a rule exhibits high support but only marginally higher confidence, it typically signifies limited reliability and an ambiguous relationship between the antecedent and consequent. Conversely, if a rule demonstrates high confidence but low support, it generally implies inadequate reliability and lacks reference value. To quantitatively characterize the efficacy of rules, additional measures such as lift and deployment capability are required.

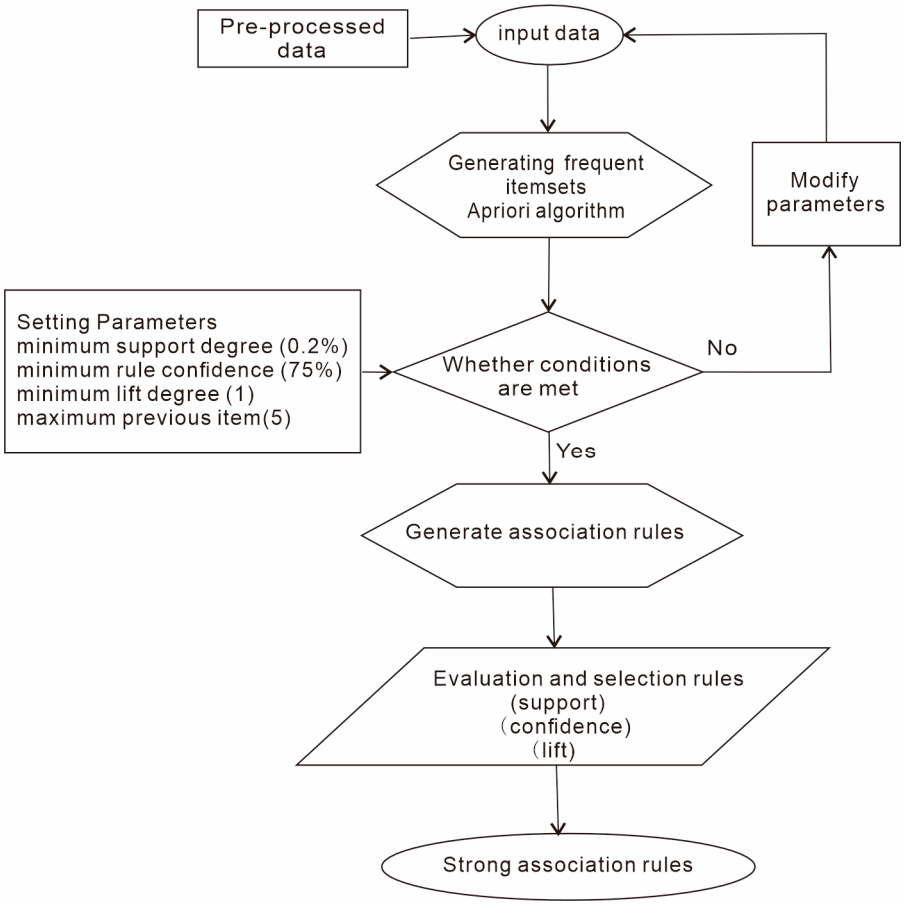


Figure 3. Schematic flow of association rule algorithm.

The lift of a rule, denoted as $L_{A\to B} = \frac{C_{A\to B}}{S_B} = \frac{P(B/A)}{P(B)}$, is defined as the conditional probability of event B given event A divided by the marginal probability of event A. In other words, the lift represents the ratio between the confidence level of a rule and the support level of its consequent. This metric quantifies the extent to which item A influences item B. When event $L_{A\to B} > 1$ occurs, it suggests that item A has a positive impact on item B. The positive impact increases proportionally with the magnitude of C. Conversely, when $L_{A\to B} < 1$, it implies that item A has a negative impact on item B [18].

The deployment capability, denoted as $D_{A\to B} = S_A - S_{A\to B}$, refers to the disparity between the support of rule antecedents and the support of rules, thereby reflecting the efficacy of these rules in practical applications. Specifically, deployment capability encompasses the tangible value, operational feasibility, and contextual relevance of rules within specific business environments.

3. Results

In this study, a total of 4919 drainage sediment geochemical data points were utilized in the Jinya-Mingshan area, encompassing seven elements (Au, Ba, Mo, Sb, V, W, Zn). An association analysis was conducted with Au as the target element. The sampling locations were strategically positioned at the terminus of the primary water system or upstream of the intersection of two water systems to effectively control the catchment area while considering uniformity and rationality. The point density distribution ranged from 4–6 points per square kilometer in clastic rock areas to 5–7 points per square kilometer in carbonate rock areas. During analysis and testing procedures, Au had a detection limit of 0.3 parts per billion (ppb) using inductively coupled plasma mass spectrometry; Mo and W had detection limits of 0.2 parts per million (ppm) and 0.3 ppm, respectively, using the same

method; Sb had a detection limit of 0.05 ppm utilizing atomic fluorescence spectrometry; Ba had a detection limit of 10 ppm; V had a detection limit of 5 ppm; and Zn had a detection limit of 4 ppm using X-ray fluorescence.

3.1. Statistical Characteristics of Elements

The statistical parameters obtained from the data analysis are presented in Table 2 and Figure 4.

Table 2. Statistical parameters of elements in stream sediment samples from the Jinya-Mingshan area.

Parameters	Minimum Value	Maximum	Average	Median	Standard Deviation	Skewness	Standard Error of Skewness	Kurtosis	Standard Error of Kurtosis
Au	0.31	734.00	5.68	2.14	28.09	18.66	0.03	405.19	0.07
Ba	10.00	3674.00	348.63	360.00	100.84	7.56	0.03	243.14	0.07
Mo	0.20	153.00	2.62	1.20	6.18	9.62	0.03	142.65	0.07
Sb	0.42	8779.00	16.05	7.53	130.12	62.59	0.03	4188.73	0.07
V	29.90	509.00	168.20	144.00	64.12	1.57	0.03	3.06	0.07
W	0.30	263.00	3.03	2.62	3.93	58.77	0.03	3881.10	0.07
Zn	30.00	1161.00	238.57	158.00	147.93	0.64	0.03	−0.75	0.07

Note: Au is in units of 10^{-9}, other elements are in units of 10^{-6}.

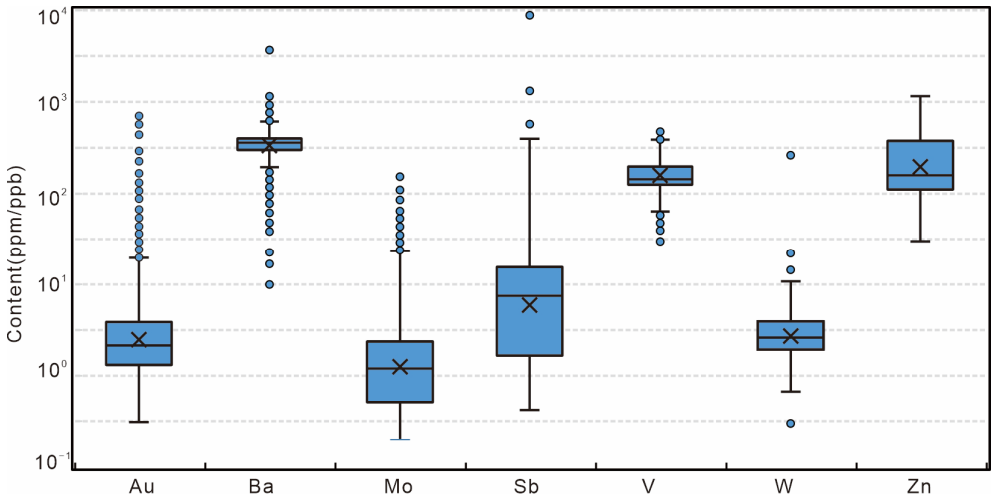


Figure 4. Box-plots of the elements in stream sediment from the Jinya-Mingshan area.

Based on the statistical analysis of the original data, it is evident that the metallogenic element Au exhibits a right-skewed distribution trend. The other six elements also demonstrate significant right-skewed distribution trends as their skewness values are greater than zero. Moreover, Ba, Mo, Sb, and W elements exhibit kurtosis values far exceeding three, indicating an extremely steep peak shape distribution pattern while V element's kurtosis value of 3.06 suggests a slightly higher peak value compared to normal distribution (middle peak state). On the contrary, Zn element's negative kurtosis (−0.75) implies flatter and more dispersed data distribution with less concentration around the mean and fewer extreme values present. The abundance and skewness of all seven elements are generally large with variation ranges in content spanning several orders of magnitude. To ensure closer adherence to positive distributions without altering relative data magnitudes, a logarithmic transformation was applied to the dataset for subsequent processing. Cluster analysis using SPSS software was conducted after taking logarithms of these elements to explore interrelationships between them (Figure 5).

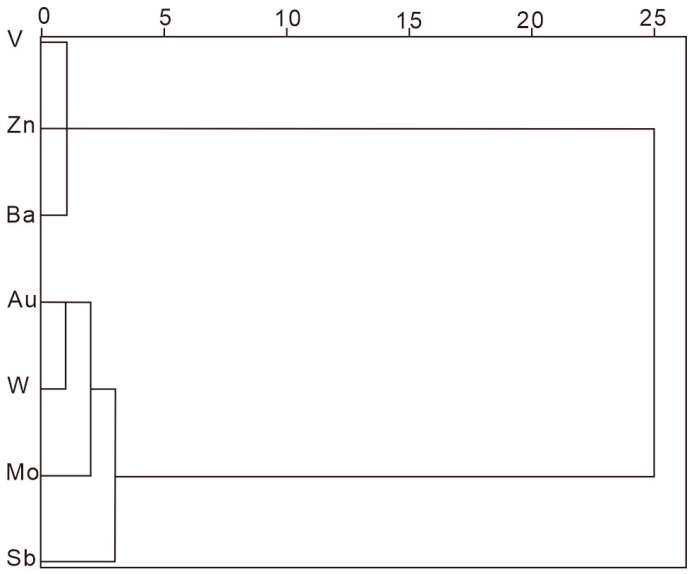


Figure 5. Dendrogram of the R-cluster analysis of the elements in stream sediment from the Jinya-Mingshan area.

According to the results of the element cluster analysis, with a distance coefficient set at 5, the seven elements can be classified into two distinct categories exhibiting strong correlations. The first category comprises Au, Mo, Sb, and W; while the second category consists of Ba, V, and Zn.

3.2. Spatial Distribution of Elements

After applying weighted inverse distance square interpolation to the logarithm-transformed data, spatial distribution diagrams were generated for each element (Figure 6). The spatial distribution patterns of the elements generally exhibit a northwest-southeast trend in high-value regions. Specifically, Au, Sb, W, V, and Zn show consistent overall spatial distribution characteristics with high-value regions primarily located in the Mingshan-Luolou area and its northwest extension. Additionally, noticeable high-value regions are observed in Jinya and its western area (Figure 6). These distributions align well with the Carboniferous Permian strata, particularly their junctions with Triassic strata (Figure 2). The Mo element predominantly exhibits high values within the Permian strata while the Ba element shows scattered high value areas that generally coincide with the distribution range of Triassic strata.

3.3. Factor Analysis

Factor analysis, a widely used statistical method, serves to reduce dimensionality and simplify complex datasets by analyzing the internal relationships among multiple variables. Through this process, a smaller set of latent variables, referred to as factors, is derived to represent the core information embedded within the original variables. The key steps in factor analysis typically involve the following: (1) determining the appropriate number of factors based on explanatory variance or characteristic roots, (2) performing factor rotation to elucidate the relationship between factors and variables, (3) interpreting and labeling each factor to comprehend its significance and role within the dataset [19,20]. Prior to conducting factor analysis, it is essential to assess whether the data are suitable for this technique by conducting Kaiser–Meyer–Olkin (KMO) test and Bartlett's sphericity test. A higher KMO value indicates greater suitability for factor analysis, while a p-value less than 0.05 in Bartlett's sphericity test suggests that the data conform to spherical distribution and

are appropriate for factor analysis. Otherwise, if these conditions are not met, it implies that the data may not be suitable for factor analysis [21].

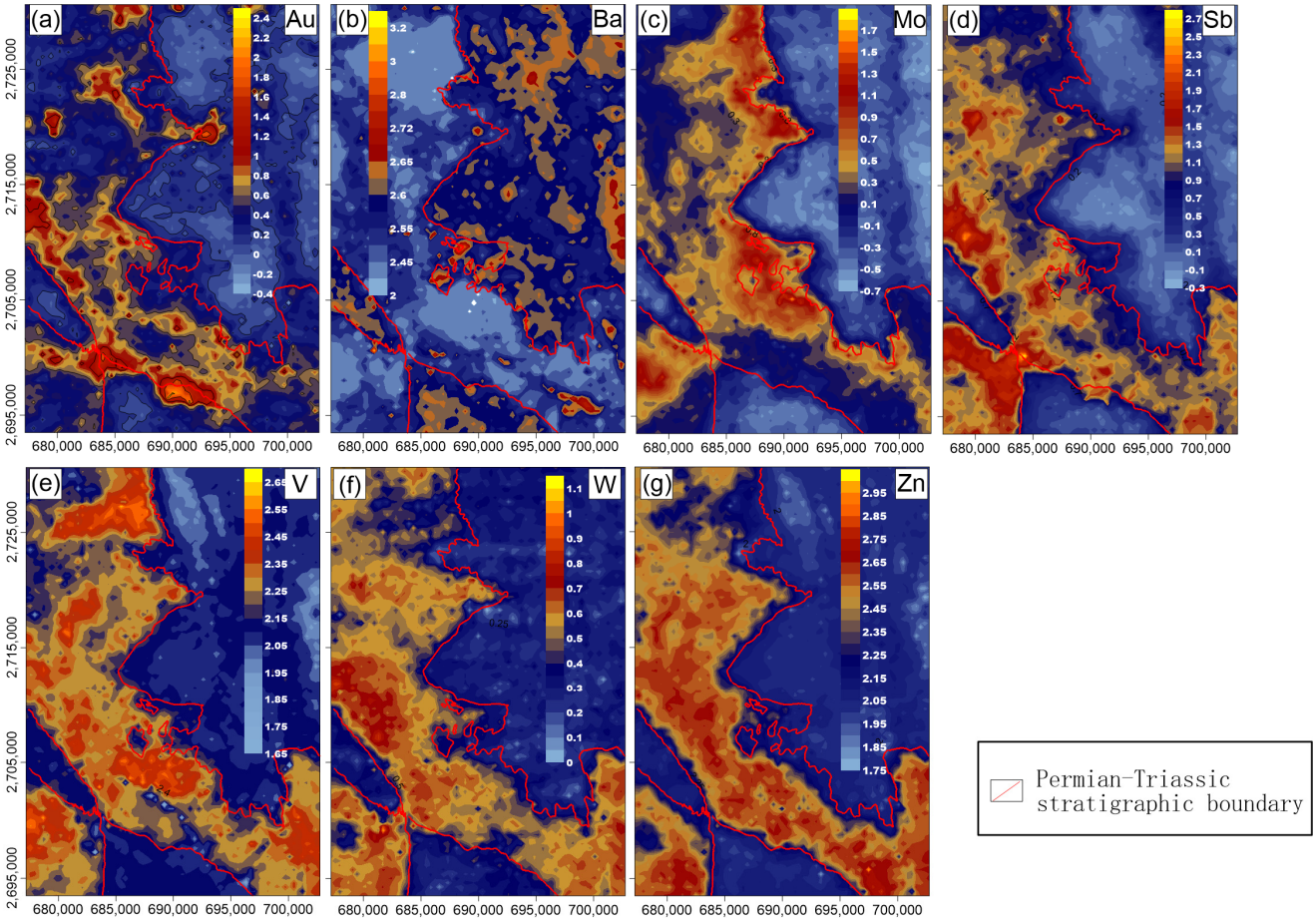


Figure 6. Spatial distribution of elements (**a**–**g**) in stream sediment from the Jinya-Mingshan area.

Based on the logarithmically transformed data of seven elements in washed sediments from the Jinya-Mingshan gold deposit area, the suitability of the data for factor analysis was confirmed by a KMO value of 0.807 and a significant probability value obtained from Bartlett's sphericity test (Table 3). The principal component extraction method was employed, resulting in the extraction of three factors with a cumulative variance contribution rate of 83.34%. Rotation was performed using Caesar's normalized maximum variance method, which converged after four iterations. The component matrix after rotation is presented in Table 4 and Figure 7.

Table 3. KMO and Bartlett tests of elements in stream sediment from the Jinya-Mingshan area.

KMO measure of suitability for sampling.		0.807
Bartlett sphere Degree test	Approximate Chi-square	21,169.240
	Degrees of Freedom	21.000
	Significance (P)	0.000

Table 4. Rotated loading coefficient matrix of the elements in stream sediment from the Jinya-Mingshan area.

Elements	Factor 1 (F1)	Factor 2 (F2)	Factor 3 (F3)
Ln(Au)	0.233	0.106	0.949
Ln(Ba)	−0.037	−0.922	−0.044
Ln(Mo)	0.489	0.620	0.318
Ln(Sb)	0.702	0.324	0.481
Ln(V)	0.741	0.424	0.140
Ln(W)	0.892	0.016	0.220
Ln(Zn)	0.914	0.083	0.159
Eigenvalue	2.969	1.536	1.328
Percentage of variance contribution	42.421	21.942	18.977
Cumulative variance contribution rate	42.421	64.363	83.340

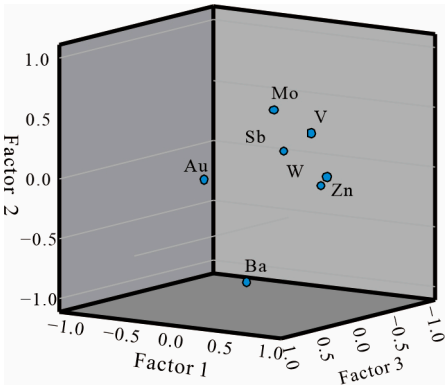


Figure 7. Rotated loading map of the elements in stream sediment from the Jinya-Mingshan area.

Factor 1 (F1) accounts for 42.421% of the total variance in the dataset and exhibits a strong positive load coefficient for Ln(Zn) (0.914), Ln(W) (0.892), Ln(V) (0.741), and Ln(Sb) (0.702). Additionally, F1 demonstrates a moderate positive load coefficient for Ln(Mo) (0.489), while showing a negative load coefficient for Ln(Ba) (−0.037). Conversely, Factor 2 (F2) explains 21.942% of the total variance and displays a relatively high negative load coefficient for Ln(Ba) (−0.922). In addition, F2 exhibits a relatively high positive loading for Ln(Mo) (0.620). Notably, the loadings for Ln(W) (0.016) and Ln(Zn) (0.083) are nearly negligible on F2, suggesting that while W and Zn contribute significantly to the first factor, their influence on the second factor is minimal. The structure of our factor analysis is well-defined as correlations between variables can be distinctly assigned to different factors, enabling us to gain better insights into which underlying concepts or constructs these factors represent. Similarly, variance explained by Factor 3 (F3) amounts to 18.977%, revealing a significant positive load coefficient for Ln(Au) (0.949) and weak positive coefficients for Ln(Mo), Ln(Sb), Ln(V), Ln(W), and Ln(Zn). Furthermore, the almost zero-load coefficient (−0.044) for Ln(Ba) suggests that element Ba contributes little explanatory power or contribution to this particular factor

The weighted inverse distance square interpolation was performed based on the factor scores of each sample, followed by the construction of an isochronous plot for each factor score (Figure 8). It can be observed from the figure that the distribution characteristics of high scores in the F1 factor are essentially consistent with the distribution patterns exhibited by elevated levels of Zn, W, V, and Sb elements. Similarly, the distribution features within the high-score region of the F2 factor align closely with those associated with increased concentrations of Mo element. Furthermore, the high-scoring region in the F3 factor

demonstrates a strong resemblance to areas exhibiting elevated values for Au element, thereby corroborating their corresponding load coefficients within each respective factor.

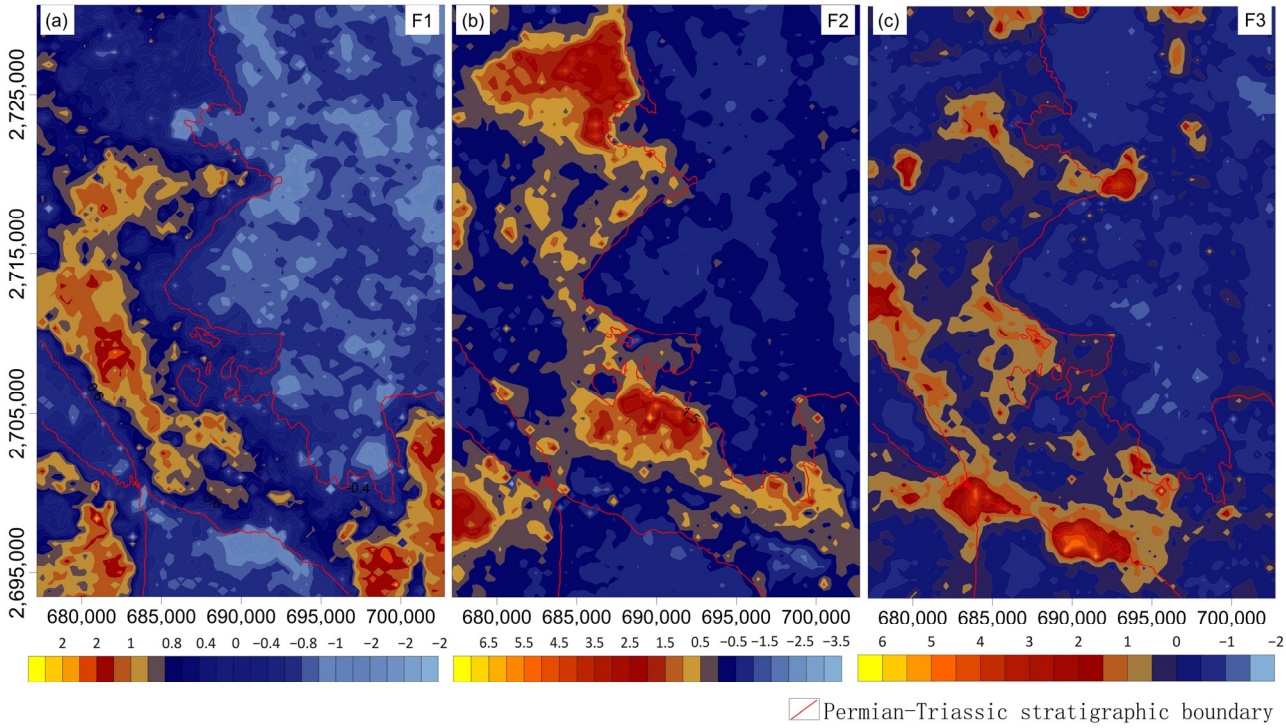


Figure 8. Spatial distribution of factor scores of stream sediment samples from the Jinya-Mingshan area, factor 1 (**a**), factor 2 (**b**), factor 3 (**c**).

3.4. Association Rule Analysis of Gold Mineralization

3.4.1. Data Classification

In this study, K-means clustering algorithm was used to transform the structured data. When K-means clustering was performed on the original geo-data, it was found that many elements have the problem of extreme imbalance in grouping, and the amount of data in different groups of the same element grouping may differ by three orders of magnitude, which is not good for the subsequent association rule algorithm analysis [13]. The monotonicity of the data obtained after logarithmic transformation does not change, which makes the various groups of elements more balanced and is conducive to the analysis of the following association rule algorithm. Therefore, this paper carries out K-mean clustering for the data obtained after logarithmic transformation of each element, and divides each element into three different category groups: high-content group, medium-content group, and low-content group. As the metallogenic target element, Au element can be divided into three categories by K-means clustering: low-content group (0.31~2.18), medium-content group (2.19~9.04) and high-content group (9.09~734.36). The corresponding samples were 2515, 2012, and 392, respectively. Considering that three-times the average content of Au in the crust (about 1.5×10^{-9}) is usually taken as the criterion for determining mineralization [22], it is believed that Au1 indicates no mineralization, Au2 indicates weak mineralization, and Au3 indicates obvious mineralization (Table 5). The other elements were also divided into three categories using the K-means clustering algorithm, and the results are shown in Table 5.

Table 5. Clustering results of element in stream sediment from the Jinya-Mingshan area.

Elements	Categories	Content Range	Sample Size	Elements	Categories	Content Range	Sample Size
Au	Au1	(0.31~2.18)	2515	V	V1	(29.87~119.1)	767
	Au2	(2.19~9.04)	2012		V2	(119.94~179.11)	2468
	Au3	(9.09~734.36)	392		V3	(179.83~557.24)	1684
Ba	Ba1	(9.99~211.03)	343	W	W1	(0.3~2.79)	2634
	Ba2	(211.88~340.02)	1674		W2	(2.8~22.22)	2284
	Ba3	(340.7~3677.54)	2902		W3	(22.24~263.22)	1
Mo	Mo1	(0.2~0.84)	1877	Zn	Zn1	(29.99~150.05)	2412
	Mo2	(0.84~3.38)	2223		Zn2	(150.96~179.11)	639
	Mo3	(3.39~153.09)	819		Zn3	(290.91~1193.92)	1868
Sb	Sb1	(0.42~3.93)	1993				
	Sb2	(3.95~20.59)	2093				
	Sb3	(20.7~8786.75)	833				

3.4.2. Association Rule Analysis

Taking Au as the target element and the other 6 elements as input items, with serial number serving as record identification, we set the minimum support degree of parameters to 0.2%, minimum confidence to 75%, minimum lift degree to 1, maximum previous item to 5, and conducted association rule analysis. Ultimately, we obtained a total of 216 association rules, among which Table 6 presents some representative rules. For further analysis purposes, we selected Rules 1, 5 and 9 as examples.

Table 6. Examples of association rules of element in stream sediment from the Jinya-Mingshan area.

Serial Number	Association Rules	Instances	Support %	Confidence %	Gain	Ability to Deploy
1	$(V1 \cap Ba2 \cap Mo1 \cap Sb1) \rightarrow Au1$	122	2.338	94.262	1.844	0.142
2	$(V1 \cap Ba2 \cap Mo1 \cap Sb1 \cap Zn1) \rightarrow Au1$	121	2.318	94.215	1.843	0.142
3	$(V1 \cap Ba2 \cap Mo1 \cap Sb1 \cap W1) \rightarrow Au1$	121	2.318	94.215	1.843	0.142
4	$(V1 \cap Mo1 \cap Sb1 \cap Zn1 \cap W1) \rightarrow Au1$	453	8.477	92.053	1.8	0.732
5	$(Ba1 \cap Zn3 \cap Mo2 \cap V2) \rightarrow Au2$	11	0.224	100	2.445	0.0
6	$(Ba1 \cap Zn3 \cap Sb2 \cap Mo2 \cap V2) \rightarrow Au2$	10	0.203	100	2.445	0.0
7	$(Ba1 \cap Mo2 \cap W2 \cap V2) \rightarrow Au2$	12	0.224	91.667	2.241	0.02
8	$(Ba1 \cap Sb2 \cap Mo2 \cap W2 \cap V2) \rightarrow Au2$	11	0.203	90.909	2.223	0.02
9	$(Sb3 \cap W2 \cap Zn1 \cap Ba3) \rightarrow Au3$	10	0.183	90.0	11.294	0.02
10	$(V1 \cap Sb3 \cap Ba2 \cap Zn1) \rightarrow Au3$	11	0.183	81.818	10.267	0.041
11	$(V1 \cap Sb3 \cap W2 \cap Zn1) \rightarrow Au3$	10	0.163	80.0	10.039	0.041
12	$(Sb3 \cap Mo2 \cap Zn1 \cap Ba3) \rightarrow Au3$	12	0.183	75.0	9.411	0.061

For association rule 1: (V1∩Ba2∩Mo1∩Sb1)→Au1, it can be seen that the previous entry of the rule is "V1∩Ba2∩Mo1∩Sb1", there are 122 instances, the support of the rule is 2.338%, the confidence is 94.262%, the gain is 1.844, and the deployment capability is 0.142%. This means that when V1, Ba2, Mo1, and Sb1 are present in the sample at the same time, the probability of Au content being Au1 is 94.262%, which is 1.844-times of Au1 under normal circumstances. According to the deployment capability, the previous item "V1∩Ba2∩Mo1∩Sb1" appears in association rule 1, but the probability that the latter item "Au1" does not appear is 0.142%. Conversely, when the element content V1, Ba2, Mo1, and Sb1 do not appear in the sample, the support rate is 97.662%, and the probability of Au2 or Au3 is 94.262%. At the same time, the confidence percentage and gain are both large, indicating a strong positive relationship between the two.

For association rule 5: (Ba1∩Zn3∩Mo2∩V2)→Au2, it can be seen that the previous entry of the rule is "Ba1∩Zn3∩Mo2∩V2", with a total of 11 instances. The support rate of the rule is 0.224%, the confidence rate is 100%, the gain is 2.445, and the deployment capability is 0.0%. This indicates that when the element content of the sample contains Ba1, Zn3, Mo2, and V2 at the same time, the probability of Au content being Au2 is 100%, which

is 2.445-times the content Au2 under normal circumstances. According to the deployment capability, the previous rule "Ba1∩Zn3∩Mo2∩V2" appears in association rule 2, but the probability that the latter rule "Au2" does not appear is 0.0%, that is, when the former rule appears, the latter rule must appear. Conversely, when element contents Ba1, Zn3, Mo2, and V2 do not appear in the sample, the support is 99.776% and the probability of Au content is 100%. Meanwhile, the confidence percentage and gain are both large, indicating a strong positive relationship between the two.

For association rule 9: (Sb3∩W2∩Zn1∩Ba3)→Au3, it can be seen that the previous entry of the rule is "Sb3∩W2∩Zn1∩Ba3". There are 10 instances, the support degree of the rule is 0.183%, the confidence is 90.0%, the gain is 11.294, and the deployment capacity is 0.02%. This indicates that when Sb3, W2, Zn1, and Ba3 appear simultaneously in the element content of the sample, the probability that the content of Au is Au3 is 90.0%, which is 11.294- times the content of Au1 under normal circumstances. According to the deployment capability, the probability of "V1∩Ba2∩Mo1∩Sb1" and the non-occurrence of the latter "Au3" in association rule 1 is 0.02%. Conversely, when element contents Sb3, W2, Zn1, and Ba3 do not appear in the sample, the support is 99.817%, and the probability of Au content is 90.0%. At the same time, the percentage of confidence and gain are both large, indicating that there is a large positive relationship between the two.

4. Discuss

4.1. Relationship Between Element Content and Au Mineralization

Within the confines of the evaluation indicators of the association rule model (support, confidence, lift, and deployability), there is a positive correlation between an item's relevance to the target element and its frequency in preceding items within generated association rules. Conversely, items with weak correlation to the target element exhibit lower frequencies or remain unchanged in preceding items within association rules. The geological model established through data mining technology using association rules can be likened to a magnifying glass that uncovers frequent co-occurrence relationships in geological datasets and reveals underlying potential value.

According to the analysis results of association rules, the instances of low-content group (L1) and medium–high-content group (M1) for each element in the pre-association term with Au1 as the post-association term were quantified at non-mineralized positions (Figure 9a). The findings revealed a significantly higher concentration of Ba, while Mo, Sb, W, and Zn exhibited significantly lower concentrations. The concentration of V remained similar. These observations indicate a strong correlation between the unmineralized region and the medium–high-content group of Ba (M1), as well as the low-content groups of Mo, Sb, W, and Zn (L1). However, there was no significant difference in correlation with both the low-content group of V (L1) and its medium–high-content group (M1).

The instances of each element in the low-content group (L2) and middle–high-content group (M2) at the mineralized site were separately quantified when Au2-3 was used as the post-association term in the pre-association term (Figure 9b). The results revealed significantly higher concentrations of Mo, Sb, V, and Zn, while Ba and W exhibited similar levels. These findings indicate a strong correlation between mineralization site and medium to high-content group of Mo, Sb, V, and Zn (M2), but no significant difference with the low-content group of Ba and W (L2) or M2.

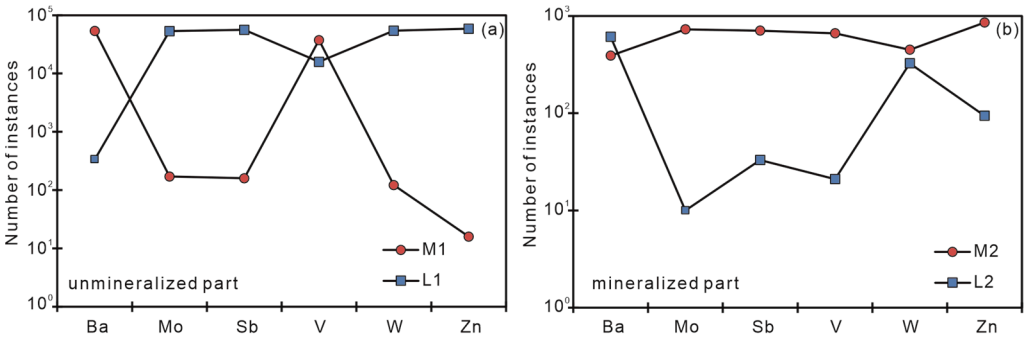


Figure 9. Number of occurrences of low- and high-content elements in stream sediments under association rules. Number of occurrences of unmineralized part (**a**), number of occurrences of mineralized part (**b**).

4.2. Mineralization Correlation Degree and Migration of Elements

The previous study investigated the strength of the correlation between the unmineralized site (Au1) and the mineralized site (Au2–3), as well as between the low-content group (L) and middle- and high-content group (M) of the other 6 elements. To further quantify the overall correlation between Au element and these 6 elements, we introduced a correlation coefficient. This coefficient can be utilized to evaluate the relationship among elements during mineralization, aiding in understanding their interactions and identifying potential areas for mineralization.

The mineralized correlation coefficient K = (M2/L2)/(M1/L1) is defined for each element, where M1, M2, L1, and L2 represent the same variables as mentioned above, with values greater than 0. When the values of M1 and L1 or M2 and L2 are relatively close, it indicates a similarity in the number of instances between the unmineralized part or mineralized part compared to the medium and high-content group. This suggests a weaker association between this element and the target element Au. A correlation coefficient K greater than 1 signifies a positive correlation between the content of an element and target element Au; higher values indicate stronger degrees of correlation and enrichment during mineralization. Conversely, when K < 1, there exists a negative correlation between this element's content and that of target element Au; smaller K values imply stronger degrees of negative correlation or loss during mineralization processes. When K ≈ 1 (close to 1), it implies no significant change in elemental content during mineralization.

Based on the degree of association between each element in the study area and the target element Au, the association strength is divided according to the value of mineralization association coefficient K, which can be divided into four items as follows (as shown in Table 7 and Figure 10): (1) Mo, Sb, and Zn are strongly positively associated elements, and their mineralization association coefficient K ∈ (7518 33,544); (2) W is a strong positive association element, whose mineralization association coefficient K = 614.87; (3) V is a weak positive correlation element, and its mineralization correlation coefficient K = 13.34; and (4) Ba is a strong negative association element with mineralization association coefficient K = 0.004.

In order to further investigate the intensity of mineralization enrichment for each element in the study area, we defined the migration enrichment coefficient λ as the ratio of average content (C2) in the mineralized part to average content (C1) in the non-mineralized part, i.e., λ = C2/C1. This coefficient is used to assess the overall migration and enrichment pattern of each element during the mineralization process (refer to Table 7, Figure 10). When C2/C1 > 1, it indicates that an element is enriched during mineralization, resulting in an increase in its content. Conversely, when C2/C1 < 1, it suggests that an element has migrated out or been consumed during the mineralization process, leading to a reduction

in its content. When C2/C1 ≈ 1, there is no significant enrichment or migration change observed for that particular element.

Table 7. Element correlation coefficients and enrichment characteristics.

Coefficients	Strong Positive Association Strongly Enriched Elements			Strong Positive Correlation with Weakly Enriched Elements	Weakly Positively Associated Weakly Enriched Elements	Strong Negative Association of Migrating Elements
	Mo	Zn	Sb	W	V	Ba
L1	53,550	58,799	56,227	54,177	15,906	338
M1	171	16	160	122	37,575	53,732
L2	10	94	33	325	21	612
M2	729	858	706	450	662	390
C1	1.65	175.2	5.75	2.42	142.05	367.18
C2	3.64	304.87	26.82	3.68	195.56	329.22
K	22,829.21	33,543.58	7518.23	614.87	13.34	0.004
Lambda.	2.2	1.74	4.67	1.52	1.38	0.89

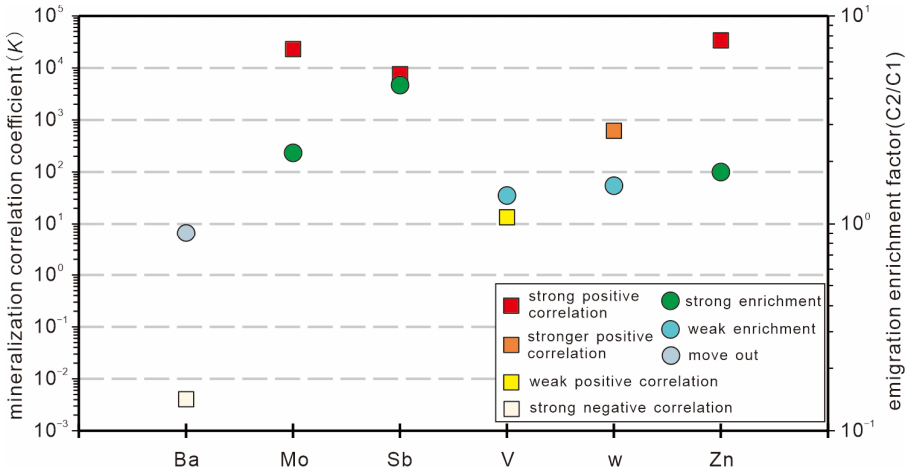


Figure 10. Correlation coefficients between selected elements and Au mineralization and elemental migration enrichment characteristics.

The average Au content in the mineralized area is approximately 10.22×10^{-9}, whereas in the unmineralized area it is approximately 1.34×10^{-9}. It can be calculated that the average content in the mineralized area is 7.63-times higher than that in the unmineralized area. Based on their enrichment coefficient λ values and actual conditions, the migration and enrichment patterns of the remaining six elements can be categorized into three groups as follows: (1) Mo, Sb, and Zn are strongly enriched elements with enrichment coefficients λ ranging from 1.74 to 4.67, indicating that their average content after mineralization is 1.74- to 4.67-times higher than before; (2) V and W are weakly enriched elements with enrichment coefficients λ ranging from 1.38 to 1.52, indicating that their average content after mineralization is 1.38- to 1.52-times higher than before; and (3) Ba is a migrated or depleted element with an enrichment coefficient λ of 0.89, suggesting that its average content after mineralization is only reduced by a factor of 0.89 compared to before.

The correlation degree of each element and mineralization in the study area can be categorized into four groups, based on the combination of the mineralization correlation coefficient K and migration enrichment coefficient λ: (1) Elements with strong positive correlation and significant enrichment: Mo, Sb, and Zn; (2) elements with weak enrichment but strong positive correlation: W; (3) elements with weak positive correlation and weak enrichment: V; and (4) migrating elements showing a strong negative association: Ba.

4.3. Relationship Between Element Content and Alteration and Mineralization

Previous studies have demonstrated that Carlin-type gold deposits in the Youjiang Basin commonly undergo alteration processes such as decarbonation, silicification, argillation, and vulcanization. The principal minerals found in gold ore comprise pyrite, arsenopyrite, a minor quantity of other metal sulfides (chalcopyrite, sphalerite, stibnite, realgar and gynozite), quartz, carbonate minerals, sericite, clay minerals, etc. [14,23].

The preceding analysis demonstrates a strong positive correlation and significant enrichment of Mo, Sb, and Zn with Au (Figure 10). The geological characteristics of the deposit reveal the presence of independent stibnite and sphalerite in the ore. Furthermore, previous studies on trace elements in sulfides from the Jinya gold deposit indicate that pyrite exhibits a high Sb content but low Zn content [3,24]. Taking this information into consideration, it can be inferred that Sb exists as isomorphic impurities or sulfides within the sulfide minerals, while Zn primarily occurs in the form of sulfides. Regarding Mo's specific form, no independent molybdenite mineral has been discovered within the studied ore deposits. Considering Mo's affinity for sulfur-bearing compounds, it is likely present as an isomorphic impurity within the sulfide minerals. In summary, elements exhibiting a strong positive association and significant enrichment with Au are closely linked to the sulfide process during mineralization. Conversely, Ba displays a strong negative correlation with Au and exhibits distinct migration characteristics (Figure 10). Given Ba's tendency to enter carbonate minerals through isomorphism, its migration may be influenced by decarbonation processes during mineralization. Based on spatial distribution patterns of strata and Ba element concentrations, Triassic strata generally exhibit high Ba contents in the study area but experience a notable decrease near Permian strata (in proximity to ore-bearing sections), where synsedimentary faults develop alongside major ore bodies (Figure 6). This further suggests that Ba migration occurred during gold mineralization and was closely associated with decarbonation processes. Element W demonstrates a robust positive correlation with Au while displaying weak enrichment characteristics (Figure 10). Considering the high field strength of element W, its inherent stability, and resistance to late geological processes, it is postulated that the weak enrichment of W is attributed to the decrease in rock density resulting from decarbonation during gold mineralization. Element V exhibits a marginal enrichment with a weak positive correlation with Au, which may be attributed to similar reasons as those for element W.

To summarize, the vulcanization process controls the distribution of Mo, Sb, and Zn during gold mineralization, leading to their enrichment in ores or altered rocks. On the other hand, decarbonation governs the behavior of Ba element, causing its migration and resulting in deficit characteristics in ores or altered rocks. Additionally, W and V elements exhibit limited enrichment due to mineralization.

4.4. Construction and Evaluation of Prospecting Index

From the perspective of association rules, in addition to Au, Mo and Sb also play a significant role in indicating mineralization and non-mineralization, which is consistent with the findings obtained through factor analysis and cluster analysis (Figure 5 and Table 4). It should be noted that association rules demonstrate Zn's effectiveness in indicating mineralization, although this relationship was not revealed by cluster analysis. Considering the distribution characteristics of elements and the geological features of ore deposits, there exists a close relationship between Au and Zn; thus, association rules provide better insights into element relationships compared to cluster analysis (Figure 5). Furthermore, association rule analysis indicates a strong negative correlation between Ba and Au elements, which aligns with geological evidence suggesting their potential as indicators for ores/non-ores; however, this significant relationship was not identified by cluster analysis or factor analysis (Figure 5 and Table 4). In summary, association rule analysis appears to outperform factor analysis and cluster analysis in revealing element relationships.

Based on the aforementioned advantages of association rule analysis, we comprehensively consider the strong positive correlation elements revealed by association rules, strong negative correlation elements, and Au elements themselves in order to construct new indicators that can more clearly indicate potential target areas of gold deposits. Considering that factor F3 in factor analysis encompasses information related to Au and strongly positively correlated elements (Table 4), we opted for replacing Au with F3 as well as incorporating the information from strongly positively correlated elements with Au. Additionally, Log(Ba) was chosen to replace the information associated with Ba element due to its positive correlation with Au while Ba exhibits a negative correlation. Consequently, in order to emphasize the comprehensive indicator function of both types of information on Au mineralization, we introduce the F3/Log(Ba) index. It is evident that existing gold deposits or ore spots are situated within or near high-value regions indicated by this new indicator, thus demonstrating its effectiveness in indicating Au mineralization. Moreover, there exists a significant agreement between the new index's high-value region and both the content of Au element and factor score (F3) (Figure 8), further affirming their collective ability to serve as reliable indicators for ore presence. However, there are some distinctions between the novel index and the other two indicators within the local area. For instance, in the three high-value regions located in the northern part of the study area (Figure 11), based on association rules, the new index suggests that the middle high-value region exhibits superior prospecting potential (the priority of target areas is determined by assessing each indicator's relative strength). Conversely, factor scores and Au content distribution indicate that the high-value region in the west demonstrates better prospecting potential (Figures 6 and 7). Considering geological characteristics and existing deposits, it can be observed that the middle–high-value area lies within Triassic ore-bearing strata in this region while the high-value area is situated near the boundary between Triassic and Permian strata; thus its prospecting potential should surpass that of the western high-value area due to the absence of gold deposits within Permian strata both inside and around our study site. In comparison with traditional indices, this new index provides a more rational selection for target areas, thereby potentially playing a significant role throughout exploration processes.

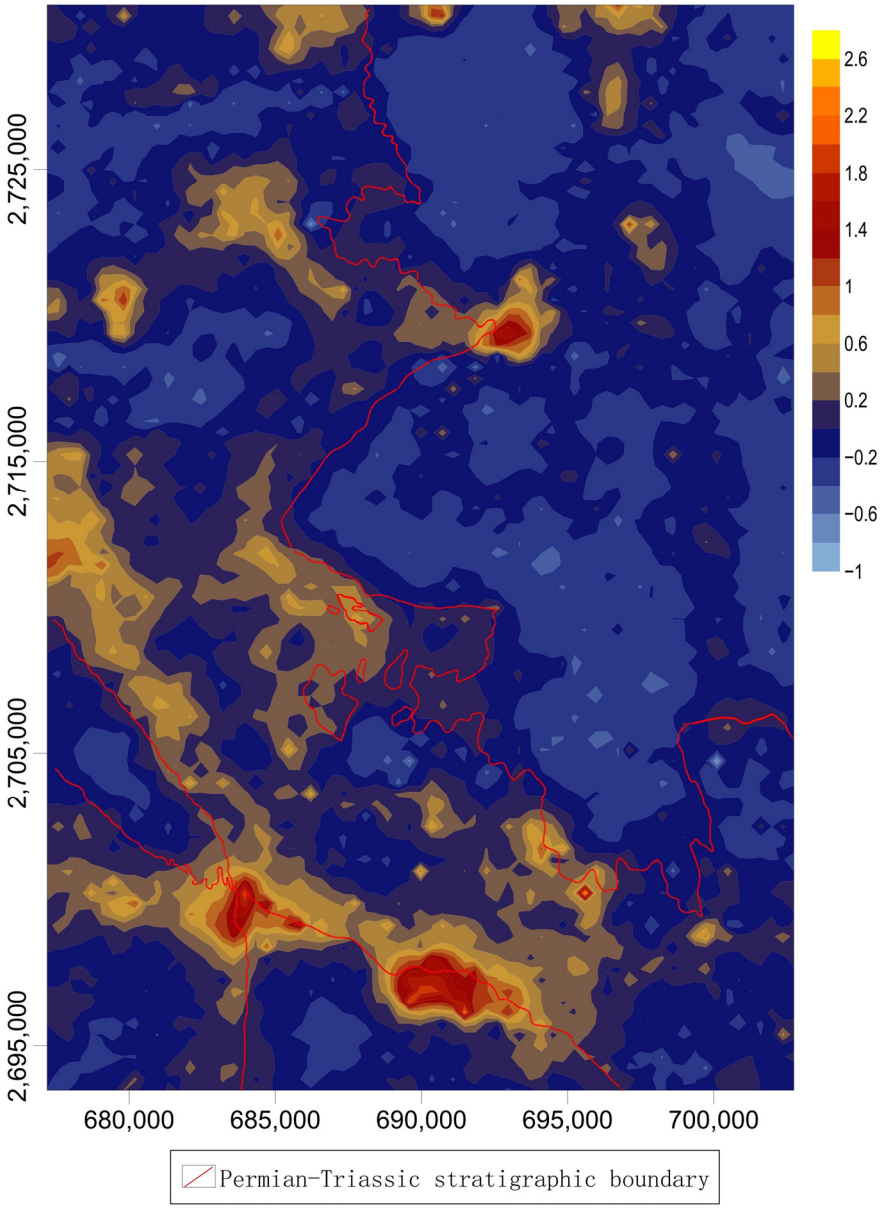


Figure 11. Spatial distribution of F3/Log(Ba) in Jinya-Mingshan area.

5. Conclusions

The Jinya-Mingshan area was selected as the study site for Carlin-type gold deposits in this study. By comparing the application effectiveness of traditional data statistical analysis methods and association rule algorithms in metallogenic prediction, the following conclusions are drawn:

(1) The element anomaly assemblage of stream sediments in the Jinya-Mingshan area can be categorized into strong positive associations and enrichments (Mo, Sb, Zn), strong positive associations and weak enrichments (W), weak positive associations and weak enrichments (V), and strong rich associations with migration tendencies (Ba). Among them, Mo, Sb, and Zn are associated with vulcanization while Ba is related to decarbonation; W and V show no significant relationship with gold mineralization;

(2) The relationships between elements excavated by association rule algorithms such as Zn and Ba exhibit better consistency with geological facts compared to those obtained through traditional methods;

(3) The element correlations extracted by association rule algorithms, together with the factor 3 derived from factor analysis, can aid in constructing more effective prospecting indices, thus demonstrating promising prospects for exploration data information mining.

Author Contributions: X.D. and G.G.; Conceptualization and methodology, Y.H.; software, W.C.; formal analysis, Z.N.; investigation, Y.H.; data curation, P.L.; writing—original draft preparation, J.M.; writing—review and editing. All authors have read and agreed to the published version of the manuscript.

Funding: This research was funded by Geological survey project of the China Geological Survey, grant number DD20242629.

Data Availability Statement: The data are contained within the article.

Acknowledgments: We appreciate the reviewers for their constructive comments and suggestions.

Conflicts of Interest: The authors declare no conflicts of interest.

References

1. Ji, X.; Chen, M.; Yang, L.; Chen, G. The relationship between Carlin-type Au mineralization and magmatism in the Youjiang Basin-a case study from the Mingshan gold deposit in northwest Guangxi, China. *Ore Geol. Rev.* **2023**, *157*, 105400. [CrossRef]
2. Li, X.; Bai, L.; Yue, Z.; Pang, B.; Wei, D. Mineralization processes involved in the formation of the Jinya Carlin-type Au deposit, northwestern Guangxi, China: Evidence from in situ trace element and S isotope geochemistry of Au-bearing zoned pyrite. *Ore Geol. Rev.* **2021**, *138*, 104376. [CrossRef]
3. Lin, Y.; Wang, Q.F.; Large, R.R.; Fougerouse, D.; Mukherjee, I.; Zhang, Q.Z.; Deng, J. Texture and geochemistry of pyrite from the Jinya, Nakuang and Gaolong gold deposits in the Youjiang Basin: Implications for basin-scale gold mineralization. *Miner. Depos.* **2022**, *57*, 1367–1390. [CrossRef]
4. Biglari, H.; Saeidi, M.; Karimyan, K.; Narooie, M.R.; Sharafi, H. Data for Factor Analysis of Hydro-geochemical Characteristics of Groundwater Resources in Iranshahr. *Data Brief* **2018**, *19*, 548–563. [CrossRef] [PubMed]
5. Huang, J.; Liu, J.; Wang, K.; Yang, Z.; Liu, X. Classification and identification of molecules through factor analysis method based on terahertz spectroscopy. *Spectrochim. Acta Part A Mol. Biomol. Spectrosc.* **2018**, *198*, 198–203. [CrossRef]
6. Harris, J.R.; Ayer, J.; Naghizadeh, M.; Smith, R.; Snyder, D.; Behnia, P.; Parsa, M.; Sherlock, R.; Trivedi, M. A study of faults in the Superior province of Ontario and Quebec using the random forest machine learning algorithm: Spatial relationship to gold mines. *Ore Geol. Rev.* **2023**, *157*, 105403. [CrossRef]
7. Liu, H.; Harris, J.; Sherlock, R.; Behnia, P.; Grunsky, E.; Naghizadeh, M.; Rubingh, K.; Tuba, G.; Roots, E.; Hill, G. Mineral prospectivity mapping using machine learning techniques for gold exploration in the Larder Lake area, Ontario, Canada. *J. Geochem. Explor.* **2023**, *253*, 107279. [CrossRef]
8. Qin, Y.Z.; Liu, L.M.; Wu, W.C. Machine Learning-Based 3D Modeling of Mineral Prospectivity Mapping in the Anqing Orefield, Eastern China. *Nat. Resour. Res.* **2021**, *30*, 3099–3120. [CrossRef]
9. Jin, X.Y.; Zhao, J.; Feng, Y.X. Calcite U-Pb dating unravels the age and hydrothermal history of the giant Shuiyindong carlin-type gold deposit in the Golden Triangle, south China. *Econ. Geol.* **2021**, *116*, 1253–1265. [CrossRef]
10. Li, X.H.; Hu, Q.F.; Xie, L.F.; Pang, B.C.; Yue, Z.H. Metallogenic Fluid Properties and Mineralization Mechanism of Jinya Gold Deposit in Northwest Guangxi. *J. Jilin Univ. (Earth Sci. Ed.)* **2023**, *53*, 840–852. [CrossRef]
11. Wang, X.L.; Cao, S.T.; Tan, Q.P.; Xie, Z.J.; Xia, Y.; Zheng, L.J.; Liu, J.Z.; Zhou, K.L.; Xiao, J.D.; Ren, T.X. Exploration Vectors and Indicators Extracted by Factor Analysis and Association Rule Algorithms at the Lintan Carlin-Type Gold Deposit, Youjiang Basin, China. *Minerals* **2024**, *14*, 492. [CrossRef]
12. Zuo, R.G. Machine learning of mineralization-related geochemical anomalies; a review of potential methods. *Nat. Resour. Res.* **2017**, *26*, 457–464. [CrossRef]
13. Cao, S.T.; Hu, R.Z.; Zhou, Y.Z.; Liu, J.Z.; Tan, Q.P.; Gao, W.; Zheng, L.J.; Song, W.F. Element enrichment pattern and prospecting method for Carlin type gold deposits based on big data association rule algorithm. *Earth Sci. Front.* **2024**, *31*, 58–72. [CrossRef]
14. Wang, Q.F.; Lin, Y.; Xu, X.J.; Santosh, M.; Wang, Y.N.; Wang, T.Y.; Chen, F.G.; Wang, R.X.; Gao, L.; Liu, X.F.; et al. Multi-stage tectonics and metallogeny associated with Phanerozoic evolution of the South China Block: A holistic perspective from the Youjiang Basin. *Earth-Sci. Rev.* **2020**, *211*, 103405. [CrossRef]
15. Xu, R.; Wunsch, D., II. Survey of clustering algorithms. *IEEE Trans. Neural Netw.* **2005**, *16*, 645–678. [CrossRef]
16. Sinaga, K.P.; Yang, M. Unsupervised K-Means Clustering Algorithm. *IEEE Access* **2020**, *8*, 80716–80727. [CrossRef]

17. Sadeghi, M.; Billay, A.; Carranza, E.J.M. Analysis and mapping of soil geochemical anomalies: Implications for bedrock mapping and gold exploration in Giyani area, South Africa. *J. Geochem. Explor.* **2015**, *154*, 180–193. [CrossRef]
18. Wei, X. *SPSS Modeler Data Mining Methods and Applications*; Publishing House of Electronics Industry: Bingjing, China, 2020.
19. Reimann, C.; Filzmoser, P.; Garrett, R.G. Factor analysis applied to regional geochemical data: Problems and possibilities. *Appl. Geochem.* **2002**, *17*, 185–206. [CrossRef]
20. Tripathi, V.S. Factor analysis in geochemical exploration. *J. Geochem. Explor.* **1979**, *11*, 263–275. [CrossRef]
21. Seyedrahimi-Niaraq, M.; Mahdiyanfar, H. Introducing a new approach of geochemical anomaly intensity index (GAII) for increasing the probability of exploration of shear zone gold mineralization. *Geochemistry* **2021**, *81*, 125830. [CrossRef]
22. Deng, J.; Wang, Q. Gold mineralization in China: Metallogenic provinces, deposit types and tectonic framework. *Gondwana Res.* **2016**, *36*, 219–274. [CrossRef]
23. Su, W.C.; Dong, W.D.; Zhang, X.C.; Shen, N.P. Carlin-Type Gold Deposits in the Dian-Qian-Gui "Golden Triangle" of Southwest China. *Rev. Econ. Geol.* **2018**, *20*, 157–185. [CrossRef]
24. Wu, W. Mineralization of the Jinya and Nakuang Carlin-like Gold Deposits in Northwest Guangxi. Master's Thesis, China University of Geosciences (Beijing), Beijing, China, 2018. Available online: https://kns.cnki.net/kcms2/article/abstract?v=ufuULlVWCsPpbJfRY-W1KVW9TWO6yg2lJ2AdTfdmWidfLCf2bfr1oJHeQvxMkOGSMa5W79YUSuctpQwYO7f3guBioPEP_fdxzAhA1jq01OumKA29wvZqJq0n-JXXK0ljGjcHBN4uWwJgpvAmuPf7BOlQGkORX_VWdS6_0z5oapPWfPB-Lsuhtiq87vg4BdosJaMo7xx4XL0=&uniplatform=NZKPT&language=CHS (accessed on 1 July 2024).

Disclaimer/Publisher's Note: The statements, opinions and data contained in all publications are solely those of the individual author(s) and contributor(s) and not of MDPI and/or the editor(s). MDPI and/or the editor(s) disclaim responsibility for any injury to people or property resulting from any ideas, methods, instructions or products referred to in the content.